Valley filter and valley valve in graphene

A. RYCERZ[1,2], J. TWORZYDŁO[3] AND C. W. J. BEENAKKER[1]*

[1]Instituut-Lorentz, Universiteit Leiden, PO Box 9506, 2300 RA Leiden, The Netherlands
[2]Marian Smoluchowski Institute of Physics, Jagiellonian University, Reymonta 4, 30-059 Kraków, Poland
[3]Institute of Theoretical Physics, Warsaw University, Hoża 69, 00-681 Warsaw, Poland
*e-mail: beenakker@lorentz.leidenuniv.nl

Published online: 18 February 2007; doi:10.1038/nphys547

The potential of graphene for carbon electronics rests on the possibilities offered by its unusual band structure to create devices that have no analogue in silicon-based electronics[1,2]. Conduction and valence bands in graphene form conically shaped valleys, touching at a point called the Dirac point. There are two inequivalent Dirac points in the Brillouin zone, related by time-reversal symmetry. Intervalley scattering is suppressed in pure samples[3–5]. The independence and degeneracy of the valley degree of freedom suggests that it might be used to control an electronic device[6], in much the same way as the electron spin is used in spintronics[7] or quantum computing[8]. A key ingredient for 'valleytronics' would be a controllable way of occupying a single valley in graphene, thereby producing a valley polarization. Here we propose such a valley filter, based on a ballistic point contact with zigzag edges. The polarity can be inverted by local application of a gate voltage to the point contact region. Two valley filters in series may function as an electrostatically controlled valley valve, representing a zero-magnetic-field counterpart to the familiar spin valve.

Earlier work[9–15] on one-dimensional (1D) conduction in graphene ribbons (long and narrow ballistic strips) has shown that they may support a propagating mode arbitrarily close to the Dirac point, and that this mode lacks the valley degeneracy of modes that propagate at higher energies. For armchair edges of the ribbon, this lowest propagating mode is constructed from states in both valleys, but for zigzag edges only a single valley contributes[9–13]. In accord with time-reversal symmetry, the mode switches from one valley to the other on changing the direction of propagation.

Here, we consider a 2D geometry consisting of a quantum point contact (QPC) in a graphene sheet. A QPC is a short and narrow constriction with a quantized conductance $G = n \times 2e^2/h$ (ref. 16). (The factor of two accounts for the spin degeneracy.) A current, I, is passed through the QPC by application of a voltage difference, V, between the wide regions on opposite sides of the constriction (see Fig. 1). The orientation of the graphene lattice is such that the constriction has zigzag edges along the direction of current flow. We demonstrate by numerical simulation that on the first conductance plateau the QPC produces a strong polarization of the valleys in the wide regions. Our finding signifies that the two valleys in graphene can be addressed individually as independent internal degrees of freedom of the conduction electrons. This is only possible in a 2D geometry, because no well-separated valleys exist in 1D.

We show that the polarization of this valley filter can be inverted by locally raising the Dirac point in the region of the constriction, by means of a gate voltage, such that the Fermi level lies in the

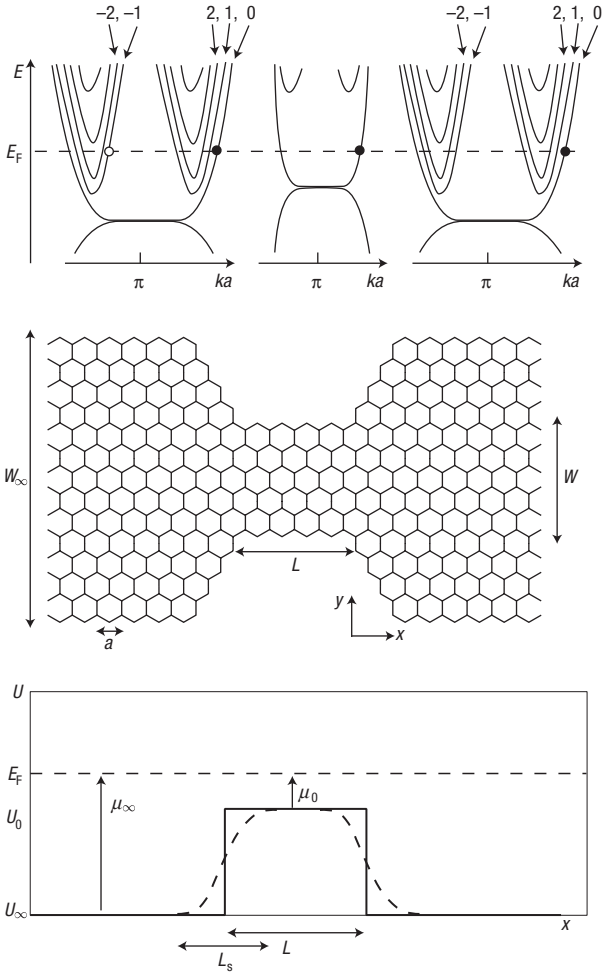

Figure 1 Schematic diagram of the valley filter. Middle panel: Honeycomb lattice of carbon atoms in a strip containing a constriction with zigzag edges. Top panel: Dispersion relation in the wide and narrow regions. An electron in the first valley (modes $n = 0, 1, 2, \ldots$) is transmitted (filled circle), whereas an electron in the second valley (modes $n = -1, -2, \ldots$) is reflected (open circle). Bottom panel: Variation of the electrostatic potential along the strip, for the two cases of an abrupt and smooth potential barrier (solid and dashed lines). The polarity of the valley filter switches when the potential height, U_0, in the constriction crosses the Fermi energy, E_F.

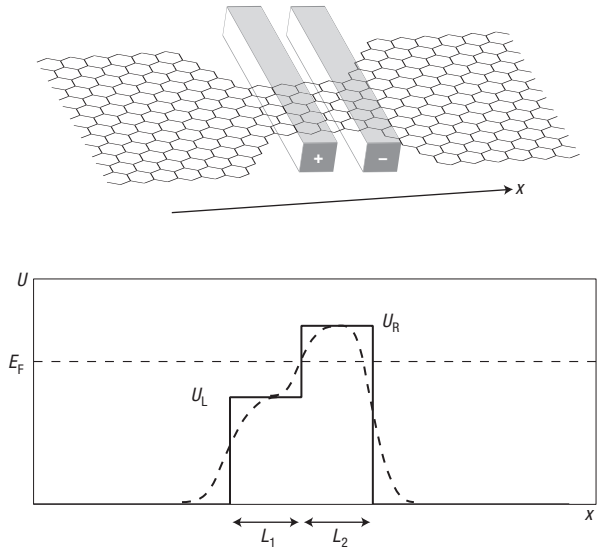

Figure 2 Schematic diagram of the valley valve (top) and corresponding potential profile (bottom). The current through the constriction is blocked if $\mu_L = E_F - U_L$ and $\mu_R = E_F - U_R$ have opposite signs.

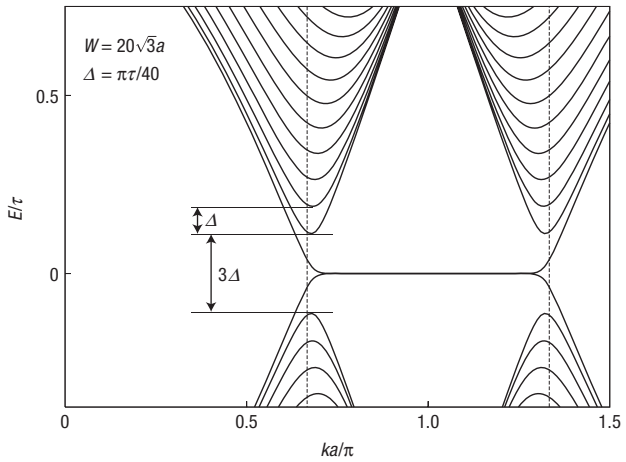

Figure 3 Dispersion relation of a graphene strip with zigzag edges. The spacing of the low-lying modes approaches $\Delta \equiv (1/2)\sqrt{3}\pi\tau a/W$ for $W/a \gg 1$. The zeroth and first modes have a larger spacing, approaching $3\Delta/2$ for $W/a \gg 1$. The vertical lines mark the valley centres at $k = 2\pi/3a$ and $4\pi/3a$.

conduction bands in the wide regions and in the valence band inside the constriction. Two valley filters in series, one acting as a polarizer and the other as an analyser, can block the current if they have the opposite polarity (see Fig. 2), demonstrating that a QPC can operate as a 'valley valve'—a purely electronic counterpart of the magneto-electronic spin valve. This extends to a 2D geometry the findings in a 1D geometry by Wakabayashi and Aoki[12]. We emphasize that their earlier work could not have demonstrated the selective population of a single valley—simply because valleys do not exist independently in 1D.

Our calculations start from the tight-binding model of graphene, with hamiltonian

$$H = \sum_{i,j} \tau_{ij} |i\rangle\langle j| + \sum_i U_i |i\rangle\langle i|.$$

The hopping matrix element $\tau_{ij} = -\tau$ if the orbitals $|i\rangle$ and $|j\rangle$ are nearest neighbours on the honeycomb lattice, otherwise $\tau_{ij} = 0$. The electrostatic potential energy $U_i = U(x_i)$ varies only along the axis of the constriction. It equals U_∞ in the wide regions and rises to U_0 inside the constriction. We smooth the stepwise increase of the potential over a length L_s, according to the function

$$\Theta_{L_s}(x) = \begin{cases} 0 & \text{if } x < -L_s/2, \\ \frac{1}{2} + \frac{1}{2}\sin(\pi x/L_s) & \text{if } |x| < L_s/2, \\ 1 & \text{if } x > L_s/2. \end{cases}$$

The potential barrier $U(x) = U_\infty + (U_0 - U_\infty)[\Theta_{L_s}(x) - \Theta_{L_s}(x-L)]$ is rectangular for $L_s = 0$ (solid line in Fig. 1, bottom panel), whereas it has a sinus shape for $L_s = L$ (dashed line).

The dispersion relation of the honeycomb lattice in a strip with zigzag edges is shown schematically in Fig. 1 (top panel) and exactly in Fig. 3. The wide regions support $2N+1$ propagating modes at the Fermi energy, E_F, which form a basis for the transmission matrix, t. Modes $n = 1, 2, \ldots, N$ lie in the first valley (with longitudinal wavevector $ka \in (\pi, 2\pi)$), whereas modes $n = -1, -2, \ldots, -N$ lie in the second valley (with $ka \in (0, \pi)$). The zeroth mode, $n = 0$, lies in a single valley fixed by the direction of propagation. The conductance of the constriction is determined by the Landauer formula

$$G = \frac{2e^2}{h} \sum_{n=-N}^{N} T_n, \qquad T_n = \sum_{m=-N}^{N} |t_{nm}|^2.$$

The valley polarization of the transmitted current is quantified by

$$P = \frac{T_0 + \sum_{n=1}^{N} (T_n - T_{-n})}{\sum_{n=-N}^{N} T_n},$$

where we consider the case (illustrated in Fig. 1) that the zeroth mode lies in the first valley. The polarization $P \in [-1, 1]$, with $P = 1$ if the transmitted current lies fully in the first valley and $P = -1$ if it lies fully in the second valley.

We have calculated the transmission matrix numerically by adapting to the honeycomb lattice the method developed by Ando for a square lattice[17]. The results are shown in Figs 4 and 5. We have fixed the width of the wide regions at $W_\infty = 70\sqrt{3}\,a$ (in units of the lattice spacing a). The electrochemical potential in the wide regions is set at $E_F - U_\infty \equiv \mu_\infty = \tau/3$, corresponding to $2N+1 = 29$ propagating modes. The narrow region has width $W = 20\sqrt{3}\,a$. We measure the electrochemical potential $E_F - U_0 \equiv \mu_0$ in the narrow region in units of the mode spacing

$$\Delta \equiv \frac{1}{2}\sqrt{3}\pi\tau a/W = \pi\hbar v/W$$

(with $v = (1/2)\sqrt{3}\tau a/\hbar = 3 \times 10^6\,\mathrm{m\,s^{-1}}$ being the energy-independent velocity in graphene). For our parameters $\Delta = \pi\tau/40$, as indicated in Fig. 3.

The operation of the valley filter is demonstrated in Fig. 4. The top panel shows the conductance, whereas the bottom panel shows the valley polarization—both as a function of the electrochemical potential, μ_0, in the narrow region. For positive μ_0, the current flows entirely within the conduction band, and we obtain plateaus of quantized conductance at odd multiples of $2e^2/h$ (as predicted by Peres *et al.*[13]). Smoothing of the potential step improves the flatness of the plateaus (compare the solid and dashed lines). The

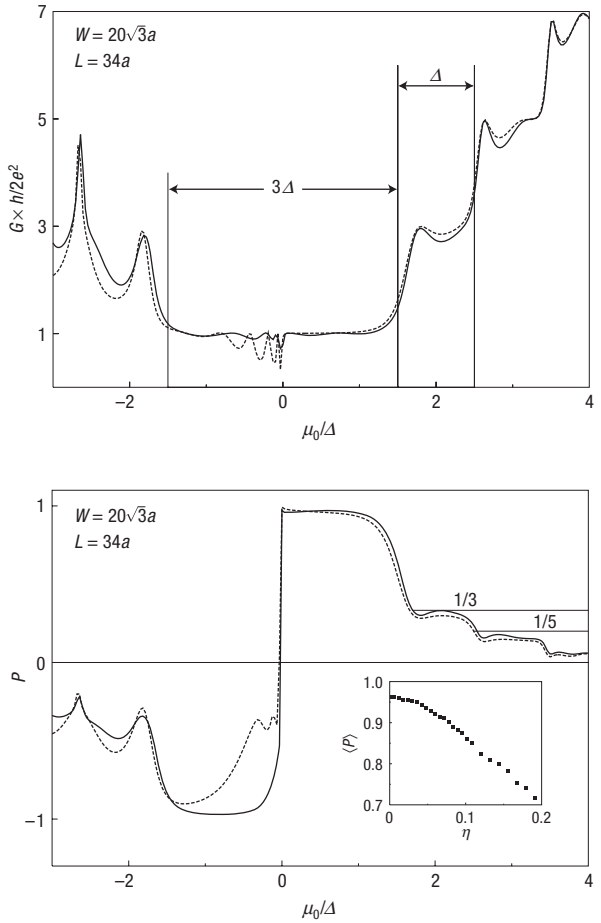

Figure 4 Conductance (top panel) and valley polarization (bottom panel) for the valley filter of Fig. 1, as a function of the electrochemical potential in the narrow region. The solid and dashed lines correspond to abrupt ($L_s = 0$) and smooth ($L_s = 8a$) potential steps, respectively. The inset in the bottom panel shows the degradation of the average valley polarization at $\mu_0 = 0.25\,\Delta$ when a randomly chosen fraction, η, of sites at the edges of the constriction contain a vacancy.

plateaus in the conductance at $G = (2n+1) \times 2e^2/h$ correspond to plateaus in the valley polarization at $P = 1/(2n+1)$. On the lowest $n = 0$ plateau, and for $0 < \mu_0 \lesssim \Delta$, the polarization is more than 95%.

For negative μ_0, the current makes a transition from the conduction band in the wide regions to the valence band in the narrow region. This interband transition has previously been studied in an unbounded system[18,19], where it leads to selective transmission at normal incidence. In the QPC studied here, we find that the interband transition destroys the conductance quantization—except on the first plateau, which remains quite flat in the entire interval $-3\Delta/2 < \mu_0 < 3\Delta/2$. The resonances at negative μ_0 are due to quasi-bound states in the valence band[20,21]. The polarity of the valley filter is inverted for negative μ_0, with some loss of quality (in particular for the smooth potential).

Because of the large Fermi wavelength at small μ_0, the quality of the valley filter is quite robust against edge imperfections. To demonstrate this, we have randomly introduced a fraction, η, of vacancies among the sites at the edges of the constriction. The resulting degradation of the polarization (averaged over a few hundred random configurations of vacancies) is shown in Fig. 4 (inset of bottom panel). The polarization remains above 95% if a few per cent of the atoms at the edge are removed, and removing as many as 1/10 of the edge atoms still leaves a polarization of 85%.

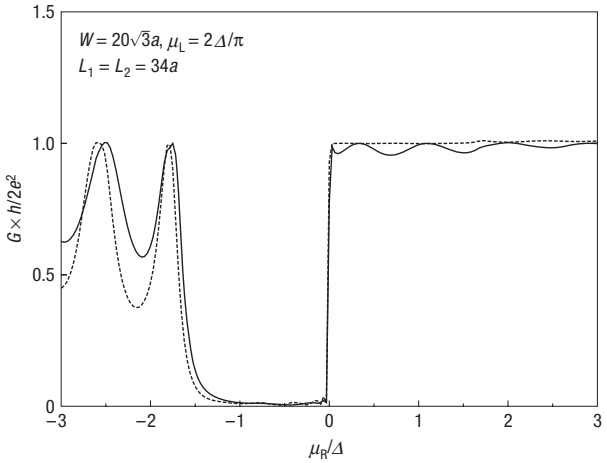

Figure 5 Conductance for the valley valve of Fig. 2 at fixed μ_L as a function of μ_R. The solid and dashed lines correspond to abrupt ($L_s = 0$) and smooth ($L_s = 8a$) potential steps, respectively.

The operation of the valley valve is demonstrated in Fig. 5. The current is blocked for $-3\Delta/2 < \mu_R < 0$ with μ_L on the first conductance plateau, so that the constriction contains two valley filters of opposite polarity in series. The switching behaviour of Fig. 5 is similar to that obtained by Wakabayashi and Aoki in a simulation of a zigzag graphene ribbon containing a potential barrier[12]. We anticipate that the experimental realization of this device will make it possible to exploit the valley degree of freedom, in addition to spin and charge degrees of freedom, as a carrier of information in carbon electronics.

Received 4 November 2006; accepted 19 January 2007; published 18 February 2007.

References

1. Novoselov, K. S. *et al.* Electric field effect in atomically thin carbon films. *Science* **306**, 666–669 (2004).
2. Berger, C. *et al.* Ultrathin epitaxial graphite: 2D electron gas properties and a route toward graphene-based nanoelectronics. *J. Phys. Chem. B* **108**, 19912–19916 (2004).
3. Morpurgo, A. F. & Guinea, F. Intervalley scattering, long-range disorder, and effective time reversal symmetry breaking in graphene. *Phys. Rev. Lett.* **97**, 196804 (2006).
4. Morozov, S. V. *et al.* Strong suppression of weak localization in graphene. *Phys. Rev. Lett.* **97**, 016801 (2006).
5. McCann, E. *et al.* Weak localisation magnetoresistance and valley symmetry in graphene. *Phys. Rev. Lett.* **97**, 146805 (2006).
6. Gunawan, O., Habib, B., De Poortere, E. P. & Shayegan, M. Quantized conductance in an AlAs two-dimensional electron system quantum point contact. *Phys. Rev. B* **74**, 155436 (2006).
7. Wolf, S. A. *et al.* Spintronics: A spin-based electronics vision for the future. *Science* **294**, 1488–1495 (2001).
8. Cerletti, V., Coish, W. A., Gywat, O. & Loss, D. Recipes for spin-based quantum computing. *Nanotechnology* **16**, R27 (2005).
9. Fujita, M., Wakabayashi, K., Nakada, K. & Kusakabe, K. Peculiar localized state at zigzag graphite edge. *J. Phys. Soc. Japan* **65**, 1920–1923 (1996).
10. Nakada, K., Fujita, M., Dresselhaus, G. & Dresselhaus, M. S. Edge state in graphene ribbons: Nanometer size effect and edge shape dependence. *Phys. Rev. B* **54**, 1795–17961 (1996).
11. Wakabayashi, K. Electronic transport properties of nanographite ribbon junctions. *Phys. Rev. B* **64**, 125428 (2001).
12. Wakabayashi, K. & Aoki, T. Electrical conductance of zigzag nanographite ribbons with locally applied gate voltage. *Int. J. Mod. Phys. B* **16**, 4897–4909 (2002).
13. Peres, N. M. R., Castro Neto, A. H. & Guinea, F. Conductance quantization in mesoscopic graphene. *Phys. Rev. B* **73**, 195411 (2006).
14. Brey, L. & Fertig, H. A. Electronic states of graphene nanoribbons studied with the Dirac equation. *Phys. Rev. B* **73**, 235411 (2006).
15. Tworzydło, J., Trauzettel, B., Titov, M., Rycerz, A. & Beenakker, C. W. J. Sub-Poissonian shot noise in graphene. *Phys. Rev. Lett.* **96**, 246802 (2006).
16. van Houten, H. & Beenakker, C. W. J. Quantum point contacts. *Phys. Today* **49** (7), 22 (1996).
17. Ando, T. Quantum point contacts in magnetic fields. *Phys. Rev. B* **44**, 8017–8027 (1991).
18. Cheianov, V. V. & Fal'ko, V. I. Selective transmission of Dirac electrons and ballistic magnetoresistance of *n-p* junctions in graphene. *Phys. Rev. B* **74**, 041403 (2006).
19. Katsnelson, M. I., Novoselov, K. S. & Geim, A. K. Chiral tunnelling and the Klein paradox in graphene. *Nature Phys.* **2**, 620–625 (2006).

20. Milton Pereira, J. Jr, Mlinar, V., Peeters, F. M. & Vasilopoulos, P. Confined states and direction-dependent transmission in graphene quantum wells. Preprint at <http://arxiv.org/abs/cond-mat/0606558> (2006).
21. Silvestrov, P. G. & Efetov, K. B. Quantum dots in graphene. *Phys. Rev. Lett.* **98**, 016802 (2007).

Acknowledgements

This research was supported by the Dutch Science Foundation NWO/FOM and by the European Community's Marie Curie Research Training Network (contract MRTN-CT-2003-504574, Fundamentals of Nanoelectronics). A.R. acknowledges a Foreign Postdoc Fellowship from the Polish Science Foundation (FNP) and support by the Polish Ministry of Science (Grant No. 1 P03B 001 29). Correspondence and requests for materials should be addressed to C.W.J.B.

Competing financial interests

The authors declare that they have no competing financial interests.